529109

PARAMETERIZATIONS OF DEPOSITIONAL GROWTH OF CLOUD ICE IN A BULK MICROPHYSICAL SCHEME

Scott A. Braun

Laboratory for Atmospheres, NASA/Goddard Space Flight Center, Greenbelt, Maryland

Brad S. Ferrier

Environmental Modeling Center, National Centers for Environmental Prediction, Washington, D. C.

Wei-Kuo Tao

Laboratory for Atmospheres, NASA/Goddard Space Flight Center, Greenbelt, Maryland

Submitted as a note to the

Journal of Applied Meteorology

March 20, 2001

Corresponding Author: Dr. Scott A. Braun, Mesoscale Atmospheric Processes Branch, NASA/GSFC, Code 912, Greenbelt, MD 20771. braun@agnes.gsfc.nasa.gov.

PARAMETERIZATIONS OF DEPOSITIONAL GROWTH OF CLOUD ICE IN A BULK MICROPHYSICAL SCHEME

Scott A. Braun, Brad S. Ferrier, and Wei-Kuo Tao

Summary

The Goddard Cumulus Ensemble model and other models use a technique for simulating clouds that includes three types of ice particles: very small cloud ice, larger snow crystals, and more dense graupel or hail. The cloud ice particles are important because they produce the large ice clouds that are blown off by thunderstorms at high levels in the atmosphere. These cloud ice particles grow by the transfer of water vapor onto the particles when the relative humidity is very high. As the ice particles grow larger, they eventually become snow. In previous versions of the cloud model, this growth process was incorrectly represented because it did not depend on the relative humidity of the air. Two corrections for this process are presented that provide the needed relative humidity dependence. Computer simulations of thunderstorm lines shows a large impact of the corrections.

ABSTRACT

The conversion of cloud ice to snow by depositional growth, designated P_{SFI}, in the Goddard Cumulus Ensemble Model cloud physics parameterization is examined. The original formulation of P_{SFI} is shown to produce excessive conversion of cloud ice to snow because of an implicit assumption that the relative humidity is 100% with respect to water even though the air may actually be quite less humid. Two possible corrections to this problem are proposed, the first involving application of a relative humidity dependent correction factor to the original formulation of P_{SFI}, and the second involving a new formulation of P_{SFI} based on the equation for depositional growth of cloud ice.

1. Introduction

The Goddard Cumulus Ensemble model (GCE, Tao and Simpson 1993; Tao and Soong 1986; Tao et al. 1993, 1996) cloud microphysics scheme is patterned after the schemes of Hsie et al. (1980; hereafter HFO) and Lin et al. (1983; hereafter LFO), but includes some modifications for cloud ice based upon the parameterizations of Rutledge and Hobbs (1983; hereafter RH). The parameterization includes three phases of ice: small cloud ice particles, larger snow crystals, and more dense graupel or hail particles. The cloud ice particles are important because they contribute significantly to the depth, width, and optical thickness of the anvil clouds generated by convection, which can significantly impact the transfer of solar and terrestrial radiation in the troposphere. An important process in the budget for cloud ice is the conversion of cloud ice to snow as the ice crystals grow by vapor deposition in the presence of cloud water, usually referred to as the Bergeron process and designated P_{SFI} (production of snow from ice) by LFO.

Examination of the conversion term reveals an inconsistency in the parameterization. Krueger et al. (1995) pointed out the problem that P_{SFI} converts ice to snow even when there is no cloud water. In fact, it converts ice to snow independent of the supersaturation with respect to ice and, as a result, produces excessive conversion of ice to snow. Since the cloud ice is assumed not to fall while snow does fall, Krueger et al. (1995) suggested that the excessive conversion of ice to snow via P_{SFI} acts as a crude parameterization of cloud ice fallout. This note describes two alternative formulations of P_{SFI} that are dependent on the supersaturation with respect to ice.

2. Numerical Model

The discussion will be supported with numerical simulations of the 10-11 June 1985 PRE-STORM[1] squall line (Johnson and Hamilton 1988; Rutledge et al. 1988; Tao et al. 1993) using the

[1] Preliminary Region Experiment for the Stormscale Operational and Research Meteorology Program (Cunning 1986).

two-dimensional version of the GCE model. The model equations are anelastic and the cloud microphysics include a parameterized Kessler-type two category liquid, three-category ice (cloud ice, snow, graupel/hail) scheme following LFO and Rutledge and Hobbs (1983). Further details about the model can be found in Tao et al. (1993, 1996).

A stretched vertical grid with 33 grid points and grid spacings from 150 m at low levels to 1000 m near model top (19 km) was used in order to maximize resolution in the lowest levels of the model. The horizontal grid consisted of 1026 grid points, the central 871 of which comprised the fine-grid area with a constant 1-km grid spacing. Outside of this region, the grid spacing was horizontally stretched with a ratio of 1.05:1 between adjacent grid points. Open lateral boundary conditions were used (Klemp and Wilhelmson 1978). A 5-km deep Rayleigh relaxation (absorbing) layer was used at the top of the model. Forward time differencing and a positive-definite advection scheme with a nonoscillatory option (Smolarkiewicz and Grabowski 1990) are used for all scalar variables (potential temperature, vapor mixing ratio, and all hydrometeor categories). A fourth-order accurate advection scheme and leapfrog time integration are used for the velocity components. The calculations use a time step of 6 s.

The model basic state is derived from the 2330 UTC 11 June 1985 sounding taken at Pratt, Kansas. This sounding is characterized by convective available potential energy of 2300 J kg^{-1}. The wind profile has been modified at upper levels to reduce the shear magnitude (see Tao et al. 1993). Convection is initiated by applying a cooling rate of up to 36 K h^{-1} over an area 65-km wide and 2.4-km deep for the first 600 s of the simulation.

Table 1 summarizes the simulations included in this study. Each case is designated by the particular formulation of PSFI (of which there are three) that is used. For consistency with the equations in Koenig (1971) and LFO and the coding of the numerical model, all equations and variables are written in cgs units.

3. Alternative formulations and numerical tests

The basis for the parameterization of the Bergeron growth process in the ice microphysics scheme is Koenig's (1971) equation for the depositional growth of ice crystals at 100% relative humidity with respect to water,

$$\frac{dm}{dt} = a_1 m^{a_2}, \tag{1}$$

where m is the crystal mass in grams and a_1 and a_2 are temperature dependent parameters [see Table 4 of Koenig (1971)]. HFO and LFO expressed the conversion of cloud ice to snow through vapor deposition as

$$\mathrm{P_{SFI}} = \frac{q_i}{\Delta t_1}, \tag{2}$$

where q_i is the cloud ice mixing ratio and Δt_1 is the time required for an ice particle to grow from some initial size m_0 to some specified size considered representative of a small snow particle, m_s. According to (1), Δt_1 can be written as

$$\Delta t_1 = \int_{m_0}^{m_s} \frac{1}{a_1}\frac{dm}{m^{a_2}} = \frac{1}{a_1(1-a_2)}\left[m_s^{(1-a_2)} - m_0^{(1-a_2)}\right] \tag{3}$$

and $\mathrm{P_{SFI}}$ can be written as

$$\mathrm{P_{SFI}} = \frac{a_1(1-a_2)q_i}{\left[m_s^{(1-a_2)} - m_0^{(1-a_2)}\right]}. \tag{4}$$

We will refer to (4) as the "original HFO" formulation of P_{SFI} and designate it with the subscript 1.

Following from Koenig's (1971) formulation for a_1 and a_2, P_{SFI1} depends only on temperature and the specified ice crystal masses m_0 and m_s, values for which can be obtained from HFO or from other mass-diameter relationships. As currently coded in the models, P_{SFI1} is independent of the supersaturation with respect to ice (i.e., 100% relative humidity with respect to water is implicit) and overestimates the conversion rate for regions with relative humidities less than 100% with respect to water. Furthermore, P_{SFI1} can be active even when the relative humidity is less than or equal to the ice saturation value.

A simple correction to the original HFO formulation of P_{SFI} is obtained by multiplying (4) by an empirically derived relative humidity factor (Hindman and Johnson 1972; Reisner et al. 1998)

$$P_{SFI2} = \frac{(q_v - q_{si})}{(q_{sw} - q_{si})} \frac{a_1(1-a_2)q_i}{\left[m_s^{(1-a_2)} - m_0^{(1-a_2)}\right]}, \quad q_v > q_{si} \tag{5}$$

where q_v, q_{si}, and q_{sw} are the vapor mixing ratio, and the saturation vapor mixing ratios over ice and water, respectively. Equation (5), which will be referred to as the "modified HFO" formulation of P_{SFI} and designated P_{SFI2}, is equivalent to Eq. (4) when the relative humidity is 100% but decreases to zero as q_v approaches the ice saturation value.

Another formulation of P_{SFI} can be derived from the ice depositional growth rate equation of RH,

$$\frac{dm}{dt} = \frac{4\overline{D}_i(S_i - 1)}{A'' + B''} \tag{6}$$

where $\overline{D}_i$ is the mean diameter of the ice crystals, $S_i = q_v/q_{si}$ is the supersaturation with respect to ice, and A'' and B'' are essentially temperature dependent parameters given below Eq. (A16) in RH. RH assumed hexagonal plate-like crystals and used the mass-diameter relationship $\overline{D}_i = 51.5m^{1/2}$, where m is the average crystal mass in grams and $\overline{D}_i$ is the crystal diameter in centimeters. Substituting m for $\overline{D}_i$ in (6) gives

$$\frac{dm}{dt} = \frac{206.2(S_i - 1)m^{1/2}}{(A'' + B'')}. \tag{7}$$

Equation (7) can be expressed in a form similar to (1) by setting $a_1 = 206.2(S_i - 1)/(A'' + B'')$ and $a_2 = 0.5$. Equation (4) then gives

$$\mathrm{P_{SFI3}} = \frac{0.5a_1 q_i}{\left[m_s^{1/2} - m_0^{1/2}\right]}. \tag{8}$$

Equation (8) will be referred to as the RH formulation of $\mathrm{P_{SFI}}$ and will be designated $\mathrm{P_{SFI3}}$. In this formulation, a_1 is both temperature and relative humidity dependent and approaches zero as the vapor mixing ratio approaches the ice saturation value. Unlike (4)-(5), $\mathrm{P_{SFI3}}$ is consistent with the cloud ice depositional growth rate (6) used in the GCE model. The values of a_1 in (8) can be compared to the values from Koenig (1971) if we consider relative humidities with respect to water of 100% (Fig. 1). Koenig's values reach a maximum near 258 K and show large variations with temperature because of assumptions of different particle habits for different temperature

regimes. Note that variations with temperature in the ice crystal growth rate caused by these variations in a_1 are offset somewhat by similar variations with temperature of a_2 coefficient in (1). The values of a_1 from P_{SFI3} are also maximum near 258 K, but show a smoother and much smaller variation with temperature because of the assumption of a single particle habit (a_2 is constant in this case).

Ice crystal masses from RH are substantially different from the masses used by HFO for the same assumed size since RH assumes hexagonal plates and HFO spherical particles. The growth equation from Koenig was formulated using particle habits (shape factor[2] and density) that varied as a function of temperature. Since spherical particles are no more valid for use at all temperatures than hexagonal plates, but RH's growth equation is based on the latter particle type, particle masses will be determined using RH's mass-diameter relationship for hexagonal plates. HFO set m_0 and m_s to the masses corresponding to 40 micron and 50 micron radius crystals. If we use the mass-diameter relationship of RH, then m_0=2.41×10^{-8} g for a 40-micron radius particle and m_s=3.76×10^{-8} g for a 50-micron particle. Krueger et al. (1995) suggested that 100 microns was a more realistic radius for small snow crystals, which gives m_s=1.51×10^{-7} g. These values are about an order of magnitude smaller than the values from HFO.

Figure 2 shows magnitudes of P_{SFI} based on the three formulations above: the original HFO formulation, P_{SFI1} (4); the modified HFO formulation, P_{SFI2} (5); and the RH formulation, P_{SFI3} (8). The calculations assume m_0 and m_s corresponding to the masses of 40- and 100-micron radius particles. The cloud ice mixing ratio is calculated assuming 40-micron sized particles in

[2] The shape factor is defined as the ratio between the maximum and minimum particle dimensions.

concentrations (n_c) that vary with temperature following Fletcher (1962), $q_i = m_0 n_c / \rho$, where q_i is the cloud ice mixing ratio and ρ is the air density. Figure 2a clearly shows the temperature dependence of the original HFO formulation and the lack of dependence upon relative humidity. The rates remain the same even when the air is subsaturated with respect to ice. The rates increase with decreasing temperature (increasing height) as a result of the increasing number concentration of cloud ice specified by the Fletcher equation.

Figure 3 shows the snow and cloud ice distributions for case PSFI1 averaged over hours 5-6 of the simulation (using output saved every 10 min). The snow field (Fig. 3a) shows an anvil slightly wider than 150 km, with large mixing ratios contained in the leading convective cells and smaller, more horizontally uniform values in the trailing stratiform region. The cloud ice distribution (Fig. 3b) is similarly characterized by large values within convective cells, but values in the trailing stratiform region are quite small, a result that will be shown to be caused by excessive conversion of cloud ice to snow by P_{SFI1}.

When the empirically derived relative humidity correction is applied (Fig. 2b, P_{SFI2}), the conversion rates for a given temperature are forced to decrease from a maximum value at 100% relative humidity with respect to water to zero at the ice saturation value. The RH formulation (Fig. 2c, P_{SFI3}) produces a qualitatively similar distribution to the modified HFO formulation, but the magnitudes are larger because, at these colder temperatures, the parameter a_1 for P_{SFI3} is larger than the Koenig value. Figure 2d shows the difference between the RH formulation and the original HFO formulation (P_{SFI1}-P_{SFI3}). For ice supersaturations exceeding 10%, the RH formulation produces larger growth rates while for small ice supersaturations (<10%) and

subsaturated conditions, the original HFO formulation produces larger growth rates, particularly at colder temperatures.

The above results imply that P_{SFI1} will cause excessive transfer of ice to snow in the upper portion of clouds that exist in conditions near saturation with respect to ice. This result is demonstrated clearly with the numerical results shown in Fig. 4, which depict the snow and cloud ice fields for case PSFI3. The snow field (Fig. 4a) shows somewhat reduced mixing ratios in the convective region compared to the case using P_{SFI1} (Fig. 3a) while the cloud ice field (Fig. 4b) shows substantially greater mixing ratios within most of the anvil, including the trailing stratiform region. In particular, P_{SFI3} leads to a broadening of the anvil cloud and an increase in cloud-top height of about 2-4 km. As in case PSFI1, case PSFI3 results in relative humidities near the ice saturation value above ~8.5 km. In case PSFI1, cloud ice was transferred to snow even though depositional growth was negligible, while in case PSFI3, no transfer of ice to snow occurred so that cloud top remained high and ice accumulated in the anvil. If the accumulation of ice in the anvil becomes excessive (as determined by either objective or subjective measures), then it can be controlled explicitly through inclusion of cloud ice fallout as opposed to having P_{SFI} cause excessive transfer of ice to snow and subsequent fallout of the snow. Using the modified HFO formulation (P_{SFI2}, not shown) yields results similar to the RH formulation (Fig. 4). Apparently, the difference in magnitude between P_{SFI2} and P_{SFI3} (Figs. 2b, c) produces only small changes to the cloud ice fields since the relative humidity tends to be near the ice saturation value.

A problem inherent in the dependence of P_{SFI} on the assumed masses m_s and m_0 is that as the difference between m_s and m_0 becomes small, the conversion rate can become very

rapid and lead to excessive depletion of cloud ice. If, on the other hand, the difference is large, then the conversion rate may become effectively negligible. Figure 5 shows the sensitivity of the different formulations of P_{SFI} in Eqs. (4, 5, 8) to the size of the larger threshold particle size, i.e., the radius of particles with mass m_s, with m_s being calculated from the mass-diameter relationship of RH. The calculations assume 90% relative humidity with respect to water (120% with respect to ice), air temperature of 243 K, and m_0 equal to the mass of a 40-micron radius particle. Significant sensitivity to the radius of the larger particle is seen between 50 and 100 microns. Figure 5 suggests that using m_s equal to the mass of a 100-micron radius particle brings the P_{SFI} terms into a range where they are less sensitive to small changes in m_s.

Krueger et al. (1995) suggested that the excessive conversion of ice to snow caused by P_{SFI1} acts like a crude fallout of cloud ice since ice is assumed not to fall while snow does. This suggestion can be tested by including a small fall speed for cloud ice in the model. The formulation of P_{SFI} assumes that the cloud ice particles are no larger than about 200 microns in diameter. Terminal velocities calculated by Heymsfield (1972) suggest maximum fall speeds of 20-30 cm s^{-1} for particles with lengths of 200 microns. Because of the uncertainty in fall velocities and their dependence on crystal habit, we simplify matters by using a constant fall velocity of 20 cm s^{-1} in the model. Figure 6 shows the snow and cloud ice fields for case PSFI3VI, which includes cloud ice fallout. The 20 cm s^{-1} fall speed has only a small effect on the snow and cloud ice distributions, the main effect being a lowering of the cloud top by at most 1 km (cf. Figs. 4 and 6). Comparison of Fig. 6 to Fig. 3 also suggests that the *excessive conversion of ice to snow by* P_{SFI1} *is not equivalent to cloud ice fallout.*

4. Conclusions

This note describes a potential problem associated with a parameterization of cloud ice depositional growth that is used in many fine-scale cloud models, including the Goddard Cumulus Ensemble (GCE) model. The problem is associated with the rate at which cloud ice is transferred to snow as a result of growth by vapor deposition, designated P_{SFI}. The formulation generally used in the parameterization is independent of relative humidity, which causes ice to be converted to snow even when the air is subsaturated with respect to ice. Two alternative formulations are presented. The first alternative simply multiplies the original formula by an empirically derived relative-humidity dependent factor so that P_{SFI} diminishes as the relative humidity approaches the ice saturation value. The second alternative formulation is derived directly from the equation for depositional growth of cloud ice used in the model. This formulation causes P_{SFI} to diminish as the relative humidity approaches the ice saturation value, but also ensures physical consistency with the parameterization of depositional growth of cloud ice used in the model. The two alternative formulations produce relatively similar results. Their main impacts include an increase of cloud-top height and a substantial increase in the cloud ice mixing ratios, particularly at upper levels in the cloud.

Acknowledgments: The Goddard Cumulus Ensemble Model development and applications are supported by the NASA Headquarters Physical Climate Program and by the NASA TRMM project. The authors are grateful to Dr. R. Kakar (NASA/HQ) for his support of this research. Acknowledgment is also made to NASA Goddard Space Flight Center for computer time used in the research.

REFERENCES

Cunning, J. B., 1986: The Oklahoma-Kansas Preliminary Regional Experiment for STORM-Central. *Bull. Amer. Meteor. Soc.*, **67**, 1478-1486.

Fletcher, N. H., 1962: *The Physics of Rain Clouds*. Cambridge University Press, 390 pp.

Heymsfield, A., 1972: Ice crystal terminal velocities. *J. Atmos. Sci.*, **29**, 1348-1357.

Hindman, E. E., and D. B. Johnson, 1972: Numerical simulation of ice particle growth in a cloud of supercooled water droplets. *J. Atmos. Sci.*, **29**, 1313-1321.

Hsie, E. Y., R. D. Farley, and H. D. Orville, 1980: Numerical simulation of ice-phase convective cloud seeding. *J. Appl. Meteor.*, **19**, 950-977.

Johnson, R. H., and P. J. Hamilton, 1988: The relationship of surface pressure features to the precipitation and airflow structure of an intense midlatitude squall line. *Mon. Wea. Rev.*, **116**, 1444-1472.

Klemp, J. B., and R. Wilhelmson, 1978: The simulation of three-dimensional convective storm dynamics. *J. Atmos. Sci.*, **35**, 1070-1096.

Koenig, L. R., 1971: numerical modeling of ice deposition. *J. Atmos Sci.*, **28**, 226-237.

Krueger, S. K., Q. Fu, K. N. Liou, and H.-N. S. Chen, 1995: Improvements of an ice-phase microphysics parameterization for use in numerical simulations of tropical convection. *J. Appl. Meteor.*, **34**, 281-287.

Lin, Y.-L., R. D. Farley, and H. D. Orville, 1983: Bulk parameterization of the snow field in a cloud model. *J. Climate Appl. Meteor.*, **22**, 1065-1092.

Reisner, J., R. M. Rasmussen, and R. T. Bruintjes, 1998: Explicit forecasting of supercooled liquid water in winter storms using the MM5 mesoscale model. *Quart. J. Roy. Meteor. Soc.*, **125**, 1071-1108.

Rutledge, S A., and P. V. Hobbs, 1983: The mesoscale and microscale structure and organization of clouds and precipitation in midlatitude cyclones. VIII: A model for the "seeder-feeder" process in warm frontal rainbands. *J. Atmos. Sci.*, **40**, 1185-1206.

————, ————, M. I. Biggerstaff, and T. Matejka, 1988: The Oklahoma-Kansas mesoscale convective system of 10-11 June 1985: Precipitation structure and single-Doppler radar analysis. *Mon. Wea. Rev.*, **116**, 1409-1430.

Smolarkiewicz, P. K., and W. W. Grabowski, 1990: The multi-dimensional positive advection transport algorithm: Nonoscillatory option. *J. Comput. Phys.*, **86**, 355-375.

Tao, W.-K., and S.-T. Soong, 1986: A study of the response of deep tropical clouds to mesoscale processes: Three-dimensional numerical experiments. *J. Atmos. Sci.*, **43**, 2653-2676.

————, and J. Simpson, 1993: The Goddard Cumulus Ensemble Model. Part I: Model description. *Terr., Atmos. Oceanic Sci.*, **4**, 35-72.

————, ————, C.-H. Sui, B. S. Ferrier, S. Lang, J. Scala, M.-D. Chou, and K. Pickering, 1993: Heating, moisture and water budgets of tropical and midlatitude squall lines: Comparisons and sensitivity to longwave radiation. *J. Atmos. Sci.*, **50**, 673-690.

————, S. Lang, J. Simpson, C.-H. Sui, B. S. Ferrier, and M.-D. Chou, 1996: Mechanisms of cloud-radiation interaction in the tropics and midlatitudes. *J. Atmos. Sci.*, **53**, 2624-2651.

Table 1. Summary of the numerical simulations.

Name	*PSFI Formulation*
PSFI1	Original HFO formulation of P_{SFI}, P_{SFI1}
PSFI2	Modified HFO formulation of P_{SFI}, P_{SFI2}
PSFI3	RH formulation of P_{SFI}, P_{SFI3}
PSFI3VI	RH formulation with 20 cm s^{-1} ice fall speed

FIGURE CAPTIONS

Figure 1. Curves of a_1 as a function of temperature. The solid line shows the values from Koenig (1971) while the dashed line shows the values for the new formulation of P_{SFI3}. For the latter values, a relative humidity of 100% has been assumed in order to be consistent with Koenig.

Figure 2. Magnitude (in units of 10^{-7} g g^{-1} s^{-1}) of the various formulations of P_{SFI}: a) the original HFO formulation (Eq. 4), b) the modified HFO formulation (Eq. 5), and c) the RH formulation (Eq. 8). Temperature is shown along the vertical axis of the plots as a proxy for height. The abscissa shows the relative humidity with respect to water. For these calculations, the temperature was assumed to vary in the vertical according to the 2330 UTC Pratt, Kansas, sounding. Solid lines in (a-c) indicate conversion rates, thick dashed lines supersaturation with respect to ice. (d) Difference between P_{SFI1} and P_{SFI3}, with positive (negative) values indicated by solid (dashed) lines.

Figure 3. Vertical cross sections of time-averaged (a) snow mixing ratio and (b) cloud ice mixing ratio for case PSFI1. Cross sections were obtained by averaging fields from hours 5-6 using output at 10-min intervals. The contour intervals are 0.1 g kg^{-1} starting at 0.01 g kg^{-1} for snow and 0.025 g kg^{-1} starting at 10^{-3} g kg^{-1} for cloud ice.

Figure 4. Same as in Fig. 3, but for case PSFI3.

Figure 5. Sensitivity of P_{SFI} to the threshold radius of snow corresponding to the mass m_s in Eqs. (4, 5, and 8).

Figure 6. Same as in Fig. 4, but for case PSFI3VI, which includes a fall velocity for cloud ice.

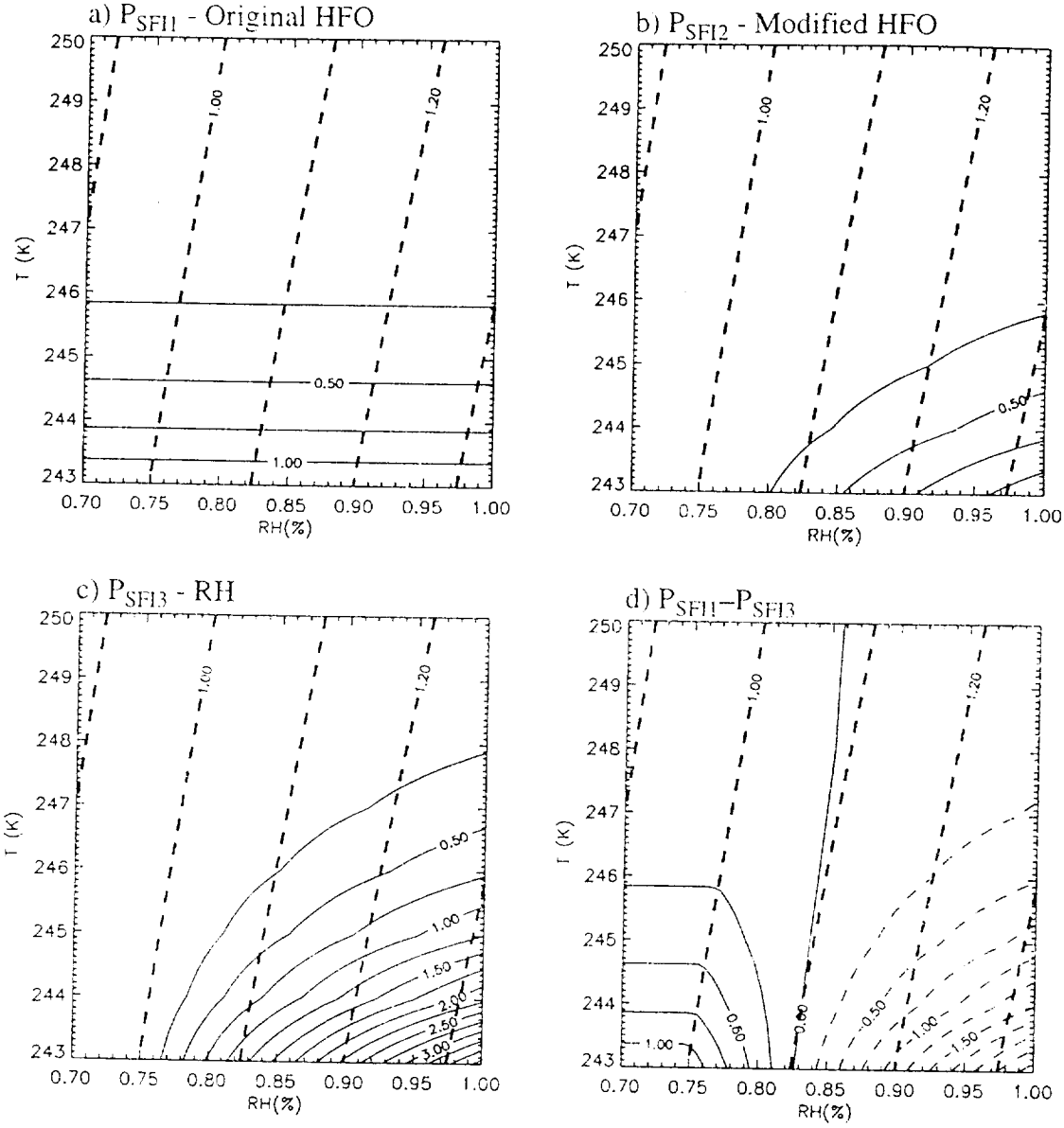

Figure 2. Magnitude (in units of 10^{-7} g g^{-1} s^{-1}) of the various formulations of PSFI: (a) the original HFO formulation (Eq. 4), (b) the modified HFO formulation (Eq. 5), and (c) the RH formulation (Eq. 8). Temperature is shown along the vertical axis of the plots as a proxy for height. For these calculations, the temperature was assumed to vary in the vertical according to the 2330 UTC Pratt, Kansas, sounding. Solid lines in (a-c) indicate conversion rates, thick dashed lines supersaturation with respect to ice (q_v/q_{si}). (d) Difference between P_{SFI1} and P_{SFI3}, with positive (negative) values indicated by solid (dashed) lines.

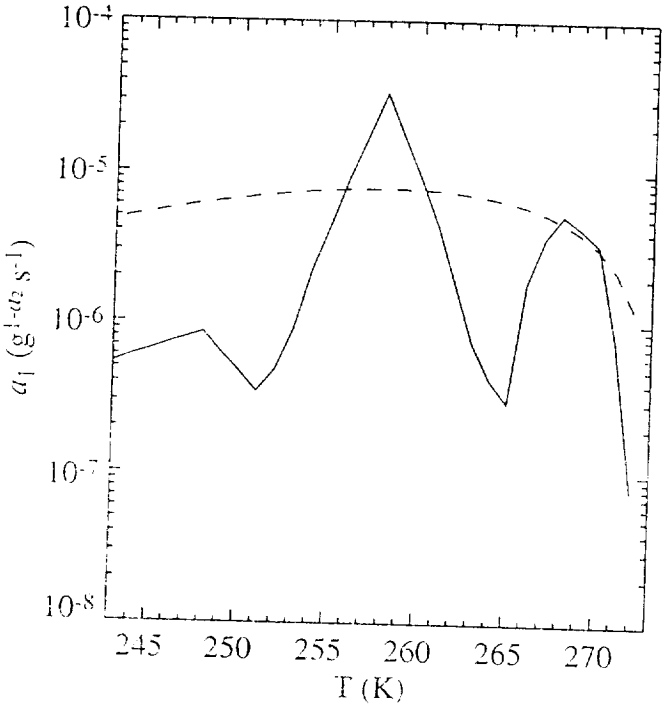

Figure 1. Curves of a_1 as a function of temperature. The solid line shows the values from Koenig (1971) while the dashed line shows the values for the new formulation of P_{SFI3}. For the latter values, a relative humidity of 100% has been assumed in order to be consistent with Koenig.